GEOPHYSICS, VOL. 74, NO. 5 (SEPTEMBER-OCTOBER 2009); P. F107–F117, 10 FIGS., 2 TABLES.
10.1190/1.3192910

Feasibility of simplified integral equation modeling of low-frequency marine CSEM with a resistive target

Shaaban A. Bakr[1] and Trond Mannseth[2]

ABSTRACT

We have assessed the accuracy of a simplified integral equation (SIE) modeling approach for marine controlled-source electromagnetics (CSEM) with low applied frequencies and a resistive target. The most computationally intensive part of rigorous integral equation (IE) modeling is the computation of the anomalous electric field within the target itself. This leads to a matrix problem with a dense coefficient matrix. It is well known that, in general, the presence of many grid cells creates a computational disadvantage for dense-matrix methods compared to sparse-matrix methods. The SIE approach replaces the dense-matrix part of rigorous IE modeling by sparse-matrix calculations based on an approximation of Maxwell's equations. The approximation is justified theoretically if a certain dimensionless parameter β is small. As opposed to approximations of the Born type, the validity of the SIE approach does not rely on the anomalous field to be small in comparison with the background field in the target region. We have calculated β for a range of parameter values typical for marine CSEM, and compared the SIE approach numerically to the rigorous IE method and to the quasi-linear (QL) and quasi-analytic (QA) approximate solutions. It is found that the SIE approach is very accurate for small β, corresponding to frequencies in the lower range of those typical for marine CSEM for petroleum exploration. In addition, the SIE approach is found to be significantly more accurate than the QL and QA approximations for small β.

INTRODUCTION

In a marine controlled-source electromagnetic (CSEM) experiment, the energy source normally is a towed horizontal electric dipole antenna. The dipole emits a low-frequency signal into the surrounding media, and stationary seafloor receivers normally record the electromagnetic (EM) signals. The marine CSEM technique, since its introduction by Cox et al. (1971), has been applied successfully to study the oceanic lithosphere and active spreading centers (Young and Cox, 1981; Cox et al., 1986; Chave et al., 1990; Evans et al., 1994; Constable and Cox, 1996; MacGregor and Sinha, 2000).

Recently, marine CSEM has become an important complementary tool for offshore petroleum exploration (Eidesmo et al., 2002; Ellingsrud et al., 2002; Tompkins, 2004; Carazzone et al., 2005; Hesthammer and Boulaenko, 2005; Srnka et al., 2005). The method exploits lossy guiding of EM energy in resistive bodies within more conductive media in an attempt to detect hydrocarbon reservoirs. For inline source-receiver geometry, the response from a thin resistive target is much more the result of galvanic effects than of inductive effects (MacGregor and Sinha, 2000; Eidesmo et al., 2002). Typically, very low source frequencies (0.05 – 1 Hz) are applied.

The actual detection of a potential petroleum reservoir is achieved through inversion of the electromagnetic data acquired in the seafloor receivers. Inversion of electromagnetic data requires repeated solves of the mathematical/numerical model in an iteration process. The computational efficiency of the solver therefore will have a great impact on the computational efficiency of the inversion. Various types of solvers, such as finite-difference (FD), finite-element (FE), and integral equation (IE) methods, have been applied. These methods have different computational advantages and disadvantages, some of which are discussed later. Hybrid methods (see, e.g., Lee et al., 1981; Best et al., 1985; Gupta et al., 1987) can be applied also.

In our work, the feasibility of using a novel approximate hybrid method as a solver for marine CSEM is assessed with respect to accuracy and range of validity. The novel method, termed simplified IE (SIE) modeling, is based on rigorous IE modeling, but it replaces the computationally most intensive part of IE modeling by an approximate method. A general motivation for why the novel method is expected to be computationally advantageous, compared to rigorous IE modeling for problems involving many grid cells in the target region, is given. A thorough and detailed comparison of computational resources, however, is left for future research.

Manuscript received by the Editor 2 May 2008; revised manuscript received 12 March 2009; published online 18 September 2009.
[1]University of Bergen, Centre for Integrated Petroleum Research, Bergen, Norway. E-mail: shaaban.bakr@cipr.uib.no.
[2]University of Bergen, Department of Mathematics and Centre for Integrated Petroleum Research, Bergen, Norway. E-mail: trond.mannseth@cipr.uib.no.

Unlike approximations of the Born type, the validity of SIE modeling does not rely on the anomalous field to be small in comparison with the background field in the target region. It does rely, however, on the galvanic effect dominating the inductive effect in the response of a thin resistive target, as discussed earlier.

The outline of the paper is as follows: We start with a brief discussion of Maxwell's equations in differential and integral forms, with emphasis on some general computational aspects of the FD and IE methods. Then we present the SIE approach to marine CSEM, and assess SIE accuracy for parameter ranges typical for petroleum exploration. Finally, we give a brief summary and conclusions and point to some future research directions.

MAXWELL'S EQUATIONS IN THE FREQUENCY DOMAIN

The CSEM radiation consists of electric $\mathbf{E}[\mathrm{V\,m^{-1}}]$ and magnetic $\mathbf{H}[\mathrm{A\,m^{-1}}]$ fields, governed by Maxwell's equations. Arbitrary components of $\mathbf{E}$, $\mathbf{H}$, are denoted E_j, H_j, respectively; $j = x,y,z$. Further, let $\mathbf{r}$ denote the spatial coordinate, Ω the entire model region, and D the target region, that is, the hydrocarbon-saturated reservoir. The conductivity distribution then can be represented as the sum $\sigma(\mathbf{r}) = \sigma^b(\mathbf{r}) + \sigma^a(\mathbf{r})$, where $\sigma^b(\mathbf{r})$ denotes the background conductivity and $\sigma^a(\mathbf{r})$ denotes the anomalous conductivity in D (that is, σ^a equals zero outside D).

Correspondingly, the expression for $\mathbf{E}(\mathbf{r})$ can be split into two parts, $\mathbf{E}(\mathbf{r}) = \mathbf{E}^b(\mathbf{r}) + \mathbf{E}^a(\mathbf{r})$, and similarly for $\mathbf{H}(\mathbf{r})$. Here, $\mathbf{E}^b$ denotes the background field, that is, the field that would have resulted if the reservoir had not been present, and $\mathbf{E}^a$ represents the part of the field caused by the existence of the anomaly.

Differential form

Assuming time variation $e^{-i\omega t}$, and neglecting displacement currents, Maxwell's equations in the frequency domain are

$$\nabla \times \mathbf{E} = i\omega\mu\mathbf{H}, \tag{1}$$

$$\nabla \times \mathbf{H} = \sigma\mathbf{E} + \mathbf{J}_e, \tag{2}$$

$$\nabla \cdot \mathbf{H} = 0,$$

$$\nabla \cdot \mathbf{E} = 0,$$

where $\mu[\mathrm{H\,m^{-1}}]$ is the magnetic permeability, $\omega[\mathrm{Hz}]$ is the angular frequency, $i = \sqrt{-1}$, $\sigma[\mathrm{S\,m^{-1}}]$ is the electric conductivity, and $\mathbf{J}_e[\mathrm{A\,m^{-1}}]$ is the source current distribution.

Integral form

For an arbitrary current-source configuration, the solution to Maxwell's equations can be written as

$$\mathbf{E}^b(\mathbf{r}') = \int_\Omega \mathcal{G}_E(\mathbf{r}'|\mathbf{r})\mathbf{J}_e(\mathbf{r})dV, \tag{3}$$

$$\mathbf{H}^b(\mathbf{r}') = \int_\Omega \mathcal{G}_H(\mathbf{r}'|\mathbf{r})\mathbf{J}_e(\mathbf{r})dV, \tag{4}$$

$$\mathbf{E}^a(\mathbf{r}') = \int_D \mathcal{G}_E(\mathbf{r}'|\mathbf{r})\sigma^a(\mathbf{r})(\mathbf{E}^b(\mathbf{r}) + \mathbf{E}^a(\mathbf{r}))dV, \tag{5}$$

$$\mathbf{H}^a(\mathbf{r}') = \int_D \mathcal{G}_H(\mathbf{r}'|\mathbf{r})\sigma^a(\mathbf{r})(\mathbf{E}^b(\mathbf{r}) + \mathbf{E}^a(\mathbf{r}))dV; \tag{6}$$

see, for example, Zhdanov (2002). Here, $\mathbf{r}'$ denotes a spatial location where $\mathbf{E}$ and $\mathbf{H}$ are to be evaluated, for instance, a receiver position, and $\mathcal{G}_{(E,H)}$ denote the Green's tensors for the electric and magnetic fields calculated for the background conductivity.

Computational aspects of differential and integral forms

We now discuss some general computational aspects of solving Maxwell's equations on differential and integral forms, respectively. First we discuss these issues in the setting of a single solve of the mathematical model (direct solver). Next we consider the situation when the direct solver is used in an inversion setting. The purpose is to explain why the SIE approach is expected to be computationally advantageous to the rigorous IE method for a sufficiently large number of grid cells in the anomalous domain D.

Direct solver

Discretization of Maxwell's equations on differential form with the FD (or FE) method results in a matrix equation for the three unknown components of $\mathbf{E}$ (or $\mathbf{H}$) in every grid cell in the computational domain Ω. With many grid cells in Ω, the coefficient matrix will be high dimensional. Because of the localized nature of differential operators, however, the coefficient matrix will be very sparse. The matrix equation for $\mathbf{E}$ in Ω must be solved once per source frequency per source position. Let W_{FD} denote the associated computational work per source frequency per source position.

For the IE method, it is convenient to split the corresponding computational work W_{IE} into two parts, $W_{\mathrm{IE}} = W_b + W_a$. The work W_b is associated with the computation of $\mathbf{E}^b$, $\mathbf{H}^b$, $\mathcal{G}_E$, and $\mathcal{G}_H$. The work W_a is associated with the computation of the anomalous fields $\mathbf{E}^a$ and $\mathbf{H}^a$.

Concerning W_b, the computational cost of calculating $\mathbf{E}^b$ and $\mathbf{H}^b$ from equations 3 and 4, when $\mathcal{G}_E$ and $\mathcal{G}_H$ are known in Ω, is low. For a horizontally stratified background conductivity, $\mathcal{G}_E$ and $\mathcal{G}_H$ can be calculated analytically, that is, at low cost. For more complex background conductivities, $\mathcal{G}_E$ and $\mathcal{G}_H$ must be calculated numerically by solving Maxwell's equations with an elementary source term. In the latter case, W_b alone can exceed W_{FD}, making the IE method an alternative that is computationally too costly. For a horizontally stratified medium, $W_b \ll W_a$, so the size of W_a compared to W_{FD} will decide whether the IE method is computationally less costly than the FD method.

Concerning W_a, if $\mathbf{E}^a$ is known in D, $\mathbf{E}^a$ and $\mathbf{H}^a$ can be found in the receivers from equations 5 and 6 at low computational cost. Therefore, the dominating part of W_a comes from computing $\mathbf{E}^a$ in D from equation 5. Discretizing this equation results in a matrix equation for the three unknown components of $\mathbf{E}^a$ in every grid cell in D. Given that the number of grid cells in D is the same as for the FD method, the coefficient matrix will not be as high dimensional as for the FD method (because Ω is larger than D), but it will be dense. The dense coefficient matrix will make the IE method computationally less suitable than the FD method for problems involving many grid cells in D, in the sense that if the number of grid cells in Ω for the FD method and the number of grid cells in D for the IE method increase by the same amount, W_a will grow much faster than W_{FD}. The same applies for storage requirements.

The purpose of this study is to assess the accuracy of an alternative method for calculating $\mathbf{E}^a$ in D that does not lead to a dense coefficient matrix, and therefore avoids the unwanted strong growth in W_a and storage requirements with the number of grid cells in D. Before proceeding to the presentation of this method, we continue the discussion about computational aspects of differential and integral forms, but now for an inversion setting.

Direct solver in an inversion setting

In an inversion setting, the direct solver (or at least part of it) is used repeatedly for different values of the unknown conductivity σ^a. The computational work W_{FD} will be approximately the same from one iteration to another, but with the IE method, the first iteration is special with respect to computational work. The computations associated with W_b are performed only in the first iteration because $\mathbf{E}^b$, $\mathbf{H}^b$, $\mathcal{G}_E$, and $\mathcal{G}_H$ are independent of σ^a. Therefore, over Γ iterations the total work for the FD method is approximately equal to ΓW_{FD}, whereas it is approximately equal to $W_b + \Gamma W_a$ for the IE method.

If $W_b \ll W_a$, as for a horizontally stratified background conductivity, the computational advantage/disadvantage of the IE method with respect to the FD method will be as for a single solve, except that it will be multiplied by Γ. Hence, any computational advantage/disadvantage of the IE with respect to the FD method will be amplified by Γ in this setting.

If W_b is not much smaller than W_a, as for a complex background conductivity, W_b necessarily cannot be neglected. If Γ is large, however, the relative importance of W_b is diminished, so that the IE method might be computationally less costly than the FD method in an inversion setting even for a complex background conductivity. A necessary (but not sufficient) requirement for this is that $W_a < W_{\mathrm{FD}}$. This means that in an inversion setting, an alternative IE method circumventing the dense-matrix problem originating from equation 5, may become computationally advantageous also for a complex background conductivity distribution.

SIMPLIFIED IE MODELING OF MARINE CSEM

We consider alternatives to equation 5 for calculation of $\mathbf{E}^a$ for low frequencies, thereby avoiding the computationally most intensive part of the IE method. First we derive a simplified equation for $\mathbf{E}^a$ from Maxwell's equations. Then we discuss how the simplified equation potentially can be used in combination with remaining parts of the IE method.

Anomalous field from a variable coefficient Poisson's equation

To find a simplifying approximation to Maxwell's equations, we first use the splitting of σ, $\mathbf{E}$, and $\mathbf{H}$ into their respective background and anomalous parts. Superposition applied to equations 1 and 2 then leads to

$$\nabla \times \mathbf{E}^b = i\omega\mu\mathbf{H}^b, \tag{7}$$

$$\nabla \times \mathbf{E}^a = i\omega\mu\mathbf{H}^a, \tag{8}$$

$$\nabla \times \mathbf{H}^b = \sigma\mathbf{E}^b + \mathbf{J}_e, \tag{9}$$

$$\nabla \times \mathbf{H}^a = \sigma\mathbf{E}^a + \sigma^a\mathbf{E}^b. \tag{10}$$

Applying the divergence operator to equation 10 results in

$$-\nabla\cdot(\sigma\mathbf{E}^a) = \nabla\cdot(\sigma^a\mathbf{E}^b). \tag{11}$$

Let $[r]$ be a characteristic length of an electromagnetic modeling problem, typically the distance from the source to a point where the solution is calculated. Then, according to Cheney et al. (1999), if the dimensionless parameter $\beta = \omega\mu\sigma[r]^2$ is much smaller than unity, the electric field can be approximated by the gradient of a scalar potential (that is, the inductive effect is negligible compared to the galvanic effect). Applying this to the anomalous electric field, and denoting the corresponding scalar potential by U^a, results in $\mathbf{E}^a \approx -\nabla U^a$ when $\beta \ll 1$. Inserting this expression for $\mathbf{E}^a$ into equation 11 results in a variable coefficient Poisson's equation for U^a,

$$\nabla\cdot(\sigma\nabla U^a) = \nabla\cdot(\sigma^a\mathbf{E}^b). \tag{12}$$

After solving for U^a, the anomalous electric field is found from

$$\mathbf{E}^a = -\nabla U^a. \tag{13}$$

Use of the Poisson's equation in simplified IE modeling

The suggested SIE modeling of marine CSEM consists of three steps. (In the description of these steps, and in the subsequent accuracy assessment of SIE modeling, the problem geometry is kept as simple as possible. This is done for convenience only; the SIE approach does not put any restrictions on the model geometry.) First, compute $\mathbf{E}^b$ in D and in the receivers, and $\mathbf{H}^b$ in the receivers, from equations 3 and 4, respectively. For the second and third steps, we consider two settings.

Setting I

The second step consists of eliminating the use of equation 5 altogether by using equations 12 and 13 to compute $\mathbf{E}^a$ both in D and directly in the receivers. (It is required to know $\mathbf{E}^a$ in D to calculate $\mathbf{H}^a$ in the receivers from equation 6.) The target D has a rectangular (x,z) cross section, and the line of receivers is located directly above the horizontal seafloor. The top surface of D is located at a distance d below the seafloor. The characteristic length $[r]$, in this setting, equals a typical distance r_i from an arbitrary point in D (i.e., the secondary source) to an arbitrary point where $\mathbf{E}^a(\mathbf{r}')$ is calculated from equations 12 and 13. In Figure 1, r_i corresponds to the distance from an arbitrary point in D to a receiver location, but r_i also can correspond to the distance from an arbitrary point in D to another arbitrary point in D.

The third step is to compute $\boldsymbol{H}^a$ in the receivers from equation 6.

Setting II

The computationally intensive part of equation 5 is to compute $\mathbf{E}^a$ in D. The subsequent use of equation 5 to compute $\mathbf{E}^a$ in the receivers when $\mathbf{E}^a$ is known in D, is not computationally intensive. The second step in setting II thus consists of eliminating the computationally intensive part of equation 5 by using equations 12 and 13 to compute $\mathbf{E}^a$ in D.

(Note that one has to solve equation 12 in a region larger than D to apply appropriate boundary conditions. Only the results within D

will be used, however, and a coarser grid can be applied at some distance from the boundary of D.) The characteristic length $[r]$, in this setting, equals a typical distance from an arbitrary point in D to another arbitrary point in D where $\mathbf{E}^a(\mathbf{r}')$ is calculated.

(Note that $[r]$ does not reflect the larger region introduced to be able to apply appropriate boundary conditions without imposing nonnegligible errors in D. This is because the results in the region outside D are not used in the calculations to obtain the solution; that is, they are not used to calculate the electromagnetic fields in the receivers. This is elaborated further in the subsection entitled "Base case.") For a rectangular region D, this distance cannot be larger than the diagonal, r_d; see Figure 2. In this study, we let $[r] = r_d$. The selection of $[r]$ is not unique, however; our selection represents a conservative choice in the sense that it will maximize β among all reasonable choices of characteristic distance for D. An alternative could be to let $[r]$ be the average distance between two arbitrary points in D.

The third step is to compute $\mathbf{E}^a$ and $\mathbf{H}^a$ in the receivers from equations 5 and 6, respectively.

Note that none of the steps in settings I or II require dense-matrix calculations.

VERIFICATION OF SIMPLIFIED IE MODELING OF MARINE CSEM

We seek to verify the novel computational schemes, SIE in setting I (SIE_I) and SIE in setting II (SIE_II), in two ways. First we assess the validity of $\beta \ll 1$ for a range of parameter values typical for marine CSEM applied to petroleum exploration. Next we compute $\mathbf{E}^a$ for such parameter values by the novel schemes and by the full IE scheme, and compare the results with respect to accuracy. A detailed comparison of computational costs is left for future work.

One reason for not considering a detailed comparison of computational costs in this study is that our numerical Poisson solver presently works in two dimensions, whereas the numerical rigorous IE solver works in three dimensions. For this reason, the size of β for typical parameter values is calculated for 2D situations. In addition, this issue has implications for how one can assess the accuracy of the SIE scheme by using numerical solutions produced by the rigorous IE solver as the benchmark. This is discussed when we explain the setup of the numerical examples. From now on, D denotes the xz-plane cross section of the anomaly; see Figures 1 and 2. We emphasize that for practical application of the SIE scheme, a 3D numerical Poisson solver is needed. A verification of the accuracy of the SIE scheme in the xz-plane is possible, however, with the presently implemented 2D solver.

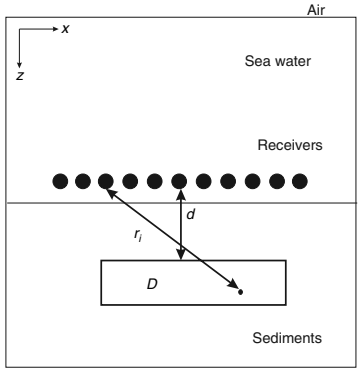

Figure 1. Sketch of model setup in setting I.

The size of β for typical parameter values

The following parameter values entering in the expression for β are used in this study: $\mu = \mu_0 = 4\pi \times 10^{-7}$ H m^{-1} (μ_0 is the free-space magnetic permeability); $\sigma^b = 1$ S m^{-1}; $\omega = 2\pi f$; and a range of frequencies, $f = \{0.05,0.1,0.3,0.5,1\}$ Hz, is considered.

Setting I

The length from an arbitrary point in D to an arbitrary receiver is not smaller than d. For reasons that will become apparent shortly, we consider d to be the characteristic length. Then the characteristic conductivity becomes σ^b, and $\beta = 2\pi f \mu_0 \sigma^b d^2$. We consider different depths, $d = \{1000,1500,2000\}$ m, and the resulting values of β are listed in Table 1.

It is seen that $\beta < 1$ only for very few of the table entries — when the frequency is very small and the reservoir depth is shallow. Note also that the values of β in Table 1 must be considered as lower bounds because d is a lower bound for $[r]$. (Note that d would be a lower bound for $[r]$ if D was a 3D conductivity structure as well.) Therefore, it seems unlikely that the SIE_I scheme will result in good approximations to the rigorous IE method, except for extremely low frequencies and shallow reservoir depths.

Setting II

For a rectangular region D, the length from an arbitrary point in D to another arbitrary point in D is not larger than $r_d = (r_h^2 + r_v^2)^{1/2}$, where r_h and r_v denote the horizontal and vertical dimensions of D, respectively; see Figure 2. For reasons that will become apparent shortly, we consider r_d to be the characteristic length. The characteristic conductivity is $\sigma_D(\sigma(\mathbf{r}),\mathbf{r} \in D)$, so β becomes equal to $2\pi f \mu_0 \sigma_D r_d^2$. We consider selected combinations of $r_h = \{1000, 3000,5000\}$ m and $r_v = \{20,50,100\}$ m, and set $\sigma_D = 0.02$ S m^{-1}. The resulting values of β are listed in Table 2.

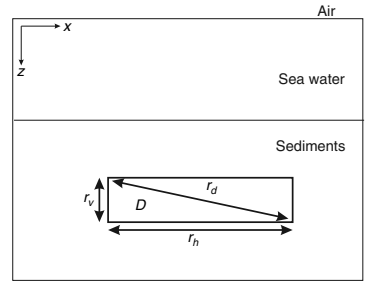

Figure 2. Sketch of model setup in setting II.

In contrast to setting I, it is seen that $\beta \ll 1$ is fulfilled for many of the table entries. Because of this, and because r_d is an upper bound for $\lceil r \rceil$, it seems likely that the SIE_{II} scheme will result in good approximations to the IE method for many frequencies and reservoir dimensions within the selected parameter ranges. (Note that in three dimensions with $r_x = r_y = r_h$, r_d would increase by less than a factor of $\sqrt{2}$. Recalling that $\lceil r \rceil = r_d$ maximizes β among all natural choices for $\lceil r \rceil$, it seems reasonable to assume that Table 2 will be informative for the 3D situation as well.)

Numerical comparison

We compare computational results obtained with the SIE method in settings I and II to the rigorous IE method (Hursán and Zhdanov, 2002). In addition, we compare to the quasi-linear (QL) approximation (Zhdanov and Fang, 1996) and the quasi-analytic (QA) approximation (Zhdanov et al., 2000) in some cases. The QL and QA approximations assume a linear relationship $\mathbf{E}^a = \lambda \mathbf{E}^b$ inside the anomalous domain, thereby avoiding the dense-matrix calculations associated with equation 5. With the QL approximation, λ is determined by solving a minimization problem. With the QA approximation, additional assumptions lead to an explicit expression for λ. We refer to Zhdanov and Fang (1996) and Zhdanov et al. (2000) for details about the QL and QA approximations, respectively.

Although a detailed comparison of computational issues is beyond the scope of this study, we give a very brief description of the numerical techniques applied to solve equation 12. Equation 12 is solved by standard finite-volume (FV) techniques on an orthogonal Cartesian grid in the xz-plane. Homogeneous boundary conditions are applied at a distance from D large enough to ensure that $\mathbf{E}^a$ in the region of interest does not change noticeably if the boundary location is moved farther away. (Alternative boundary conditions can be applied. It is possible, for instance, to apply boundary conditions generated with the QA approximation on a boundary much closer to the anomalous conductivity. This will decrease the computational effort in solving the Poisson's equation significantly, particularly in three dimensions. However, we do not pursue this issue further in this study because we are not concerned with a comparison of computational efficiencies.) The grid-cell size varies and typically is smaller within D than outside D. Care is taken, however, to apply small grid cells both inside and outside D in the vicinity of its boundary. As is well known, FV techniques require σ to be evaluated at cell edges, whereas it is known only in grid-cell centers from its discretization. For this computation, we apply the standard technique of distance-weighted harmonic averaging of neighboring grid-cell values.

All test models have vertical cross sections consisting of a homogeneous half-space under a 1000-m-thick seawater column with electric conductivity 3.33 S m^{-1}. The 3D conductivity anomaly has uniform rectangular cross sections. The source is a 100-m-long, 1000-A, x-directed horizontal electric dipole in the xz-plane, whose center location is 100 m above the seafloor and 3000 m to the left of the center of D. The applied frequencies are $f = \{0.05, 0.1, 0.3, 0.5, 1\}$ Hz. Unless otherwise stated, the homogeneous half-space has electric conductivity $\sigma^b = 1$ S m^{-1}.

Because our Poisson solver presently works in two dimensions and the rigorous IE solver, as well as the QL and QA approximate solvers, work in three dimensions, some extra care must be taken when conducting numerical comparisons of accuracy. Therefore, the modeled conductivity anomaly is given a very large extension in the y-direction to mimic a 2D situation. (The y-direction extension is selected so that the results in the xz-plane do not change noticeably when increasing it further.)

With the SIE method, $\mathbf{E}^b$ is computed in three dimensions using equation 3. The components E_x^b and E_z^b in D then are extracted and used as input to equation 12. All calculations with equations 12 and 13 are performed in the xz-plane. With the rigorous IE method, as well as with the QL and QA approximations, results within the anomaly and in the receivers can be computed in a standard fashion from equations 3–6. The components E_x^a and E_z^a in D can then be extracted from the anomaly results and compared to the corresponding SIE results.

In setting I, we compare only E_x^a and E_z^a in the receivers (which are distributed along the x-axis; see Figure 1) to rigorous IE results. The scheme SIE_{I} then computes E_x^a and E_z^a in the receivers from equations 12 and 13. Because magnetic fields in the receivers are not compared, there is no need to compute $\mathbf{E}^a$ in the anomaly.

In setting II, E_x^a and E_z^a in D are compared. (We choose, however, to show results for E_z^a only, because E_z^a typically is orders of magnitude stronger than E_x^a in D.) Results in the receivers are not compared because all involved methods apply the same equations (equations 5 and 6) to propagate the fields from the anomaly to the receivers.

The results to be shown are the amplitude of the anomalous electric field $|E_j^a|$, the pointwise relative error between the rigorous IE and SIE methods

$$\theta_j(\mathbf{r}_i) = \frac{\left||E_j^a(\mathbf{r}_i)|^{\text{IE}} - |E_j^a(\mathbf{r}_i)|^{\text{SIE}}\right|}{|E_j^a(\mathbf{r}_i)|^{\text{IE}}}, \tag{14}$$

Table 1. The size of β for different depths d and frequency f in setting I.

f/d	1000	1500	2000
0.05	0.3948	0.8883	1.5791
0.1	0.7896	1.7765	3.1583
0.3	2.3687	5.3296	9.4748
0.5	3.9478	8.8826	15.7914
1.0	7.8957	17.7653	31.5827

Table 2. The size of β for different horizontal r_h and vertical r_v dimensions of the target D and frequency f in setting II.

r_v	100	50	50	50	20
f/r_h	3000	5000	3000	1000	3000
0.05	0.0711	0.1974	0.0711	0.0079	0.0711
0.1	0.1423	0.3948	0.1422	0.0158	0.1421
0.3	0.4268	1.1845	0.4265	0.0475	0.4264
0.5	0.7114	1.9741	0.7108	0.0792	0.7106
1.0	1.4228	3.9482	1.4216	0.1583	1.4213

and the mean relative error

$$\gamma_j = \frac{1}{N}\sum_{i=1}^{N} \theta_j(\mathbf{r}_i), \tag{15}$$

where $\mathbf{r}_i$ denotes an arbitrary grid cell, N denotes the number of grid cells, and $j = x,z$.

Setting I

The results are obtained in an array of electric receivers located 10 m above the seafloor, along the line between $(x,y) = (-3,0)$ km and $(x,y) = (3,0)$ km. The electric conductivity in D is selected as $\sigma_D = 0.01$ S m^{-1}, and the dimensions and location of D are selected as $r_v = 50$ m, $r_h = 3000$ m, and $d = 1500$ m.

Figure 3a shows results for $|E_x^a|$ where $f = 0.3$ Hz, and Figure 3b shows results for $|E_z^a|$ where $f = 0.05$ Hz. In both plots, the dash-dot line corresponds to the rigorous IE method, and the solid line corresponds to the SIE_I method. The frequencies are selected to indicate where the SIE_I method ceases to be a good approximation.

Figure 3c and d shows γ_x and γ_z as functions of f. Figure 3e and f shows γ_x and γ_z as functions of β. The solid lines correspond to $d = 1000$ m, the dash-dot lines correspond to $d = 1500$ m, and the dashed lines correspond to $d = 2000$ m. Figure 3 illustrates that the SIE_I scheme is a good approximation to the IE method only for extremely low frequencies and fairly shallow reservoirs, in correspondence with Table 1.

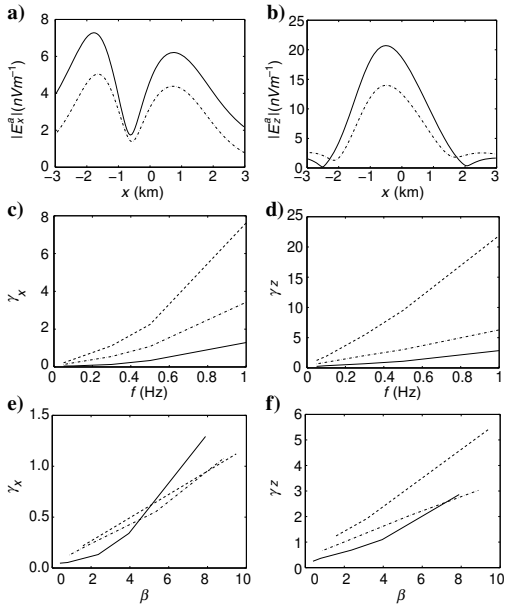

Figure 3. The amplitudes (a) $|E_x^a|$ for $f = 0.3$ Hz and (b) $|E_z^a|$ for $f = 0.05$ Hz. In (a) and (b), the dash-dot line corresponds to the IE method and the solid line corresponds to the SIE_I scheme. The mean relative errors, (c) γ_x, and (d) γ_z, as functions of f. The mean relative errors, (e) γ_x and (f) γ_z, as functions of β. In (c, d, e, and f), the solid lines correspond to $d = 1000$ m, the dash-dot lines correspond to $d = 1500$ m, and the dashed lines correspond to $d = 2000$ m.

Setting II

The depth below the seafloor is selected as 1500 m, except in the last case studied. The values of r_h, r_v, and σ_D are specified further in the description of the different cases studied. All figures shown for the different cases illustrate features of the amplitude of the vertical component of the anomalous electric field $|E_z^a|$. Typically, E_z^a represents the stronger response within D to the conductivity anomaly. One type of plot will show filled contours of $|E_z^a|$ as a function of location in D for a specific set of parameter values. For all such plots, $f = 0.1$ Hz. For the first three cases, we compare the SIE_{II} scheme to the rigorous IE method, and to the QL and QA approximations, using this type of plot.

Base case. — The dimensions of D are selected as $r_v = 50$ m and $r_h = 3000$ m, and the electric conductivity in D is selected as $\sigma_D = 0.02$ S m^{-1}.

Figure 4 shows θ_z for selected values of x when z is fixed at 2525 m, corresponding to midway between the horizontal boundaries of D. Clearly, when moving far enough away from D, the solution to equations 12 and 13 ceases to be a good approximation to the anomalous electric field obtained from Maxwell's equations. Fortunately, the SIE_{II} method uses only the field inside D where the accuracy seems very good.

Figure 5a-d shows filled contours of $|E_z^a|^{IE}$, $|E_z^a|^{SIE}$, $|E_z^a|^{QL}$, and $|E_z^a|^{QA}$ as functions of location in D, respectively. The accuracy of the SIE_{II} method for $f = 0.1$ Hz seems very good, and significantly better than the accuracies of the QL and QA approximations, respectively.

Perturbed reservoir conductivity. — The dimensions of D are selected as for the base case, $\{r_h,r_v\} = \{3000,50\}$ m. Figure 6a-d shows filled contours of $|E_z^a|^{IE}$, $|E_z^a|^{SIE}$, $|E_z^a|^{QL}$, and $|E_z^a|^{QA}$ as functions of location in D for $\sigma_D = 0.05$ S m^{-1}, respectively. The accuracies of the SIE_{II}, QL, and QA methods for $f = 0.1$ Hz are very similar to their respective accuracies in the base case.

Perturbed background conductivity. — The dimensions and the conductivity of D are selected as for the base case, $\{r_h,r_v\} = \{3000,50\}$ m and $\sigma_D = 0.02$ S m^{-1}. Figure 7a-d shows filled contours of $|E_z^a|^{IE}$, $|E_z^a|^{SIE}$, $|E_z^a|^{QL}$, and $|E_z^a|^{QA}$ as functions of location in D for $\sigma^b = 0.3$ S m^{-1}, respectively. The accuracies of the SIE_{II}, QL, and QA methods for $f = 0.1$ Hz are very similar to their respective

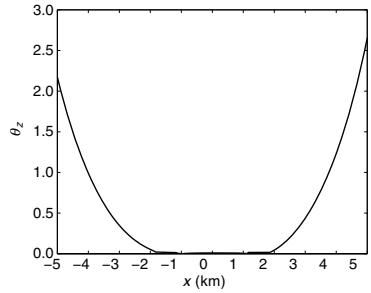

Figure 4. The pointwise relative error θ_z for the base case as a function of x when $z = 2525$ m. The extension of D in the x-direction is from -1.5 km to 1.5 km.

accuracies in the base case.

For the remaining cases, only comparisons between the SIE method and rigorous IE method are shown. (The performances of QL and QA approximations were similar to their respective performances in the previous cases.) One type of plot will show filled contours of $|E_z^a|$ as a function of location in D for a specific set of parameter values. A second type of plot will show γ_z as a function of frequency f. A third type of plot will show γ_z as a function of $\beta(f)$ when f varies.

Perturbed vertical extension. — The horizontal dimension and the conductivity of D are selected as for the base case, $r_h = 3000$ m and $\sigma_D = 0.02$ S m^{-1}. Figure 8a and c shows filled contours of $|E_z^a|^{\mathrm{IE}}$ as a function of location in D for $r_v = \{20,100\}$ m, respectively. Figure 8b and d shows filled contours of $|E_z^a|^{\mathrm{SIE}}$ as a function of location in D for $r_v = \{20,100\}$ m, respectively. The accuracy of the $\mathrm{SIE_{II}}$ method for $f = 0.1$ Hz is as good as in the base case. The solid curves in Figure 8e and f show γ_z as a function of f and β, respectively, for $r_v = 50$ m. The mean relative error γ_z increases with f and with β, but is smaller than 25% for $f \leq 0.5$, corresponding approximately to $\beta \leq 0.7$. The dash-dot curves in Figure 8e and f show γ_z as a function of f and β, respectively, for $r_v = 20$ m. The dashed curves in Figure 8e and f show γ_z as a function of f and β, respectively, for $r_v = 100$ m. The variation of γ_z with f and β is similar to that in the base case. From Table 2, it is seen that β varies only slightly with r_v within the selected ranges for r_v and r_h.

Perturbed horizontal extension. — The vertical dimension and the conductivity of D are selected as for the base case, $r_v = 50$ m and $\sigma_D = 0.02$ S m^{-1}. Figure 9a and c shows filled contours of $|E_z^a|^{\mathrm{IE}}$ as a function of location in D for $r_h = \{1000,5000\}$ m, respectively. Figure 9b and d shows filled contours of $|E_z^a|^{\mathrm{SIE}}$ as a function of location in D for $r_h = \{1000,5000\}$ m, respectively. The accuracy of the $\mathrm{SIE_{II}}$ method for $f = 0.1$ Hz is as good as in the base case. The dash-dot curves in Figure 9e and f shows γ_z as a function of f and β, respectively, for $r_h = 1000$ m. The dashed curves in Figure 9e and f show γ_z as a function of f and β, respectively, for $r_h = 5000$ m. Because β is proportional to r_d^2, it changes significantly when r_h varies from 1000 m to 5000 m. Therefore, the horizontal ranges for the curves in Figure 9f also are very different. The variation of γ_z with f and β changes somewhat with r_h. The γ_z is smaller than 25% for β as large as 2 when $r_h = 5000$ m.

Perturbed depth below the seafloor. — The dimensions and the conductivity of D are selected as for the base case, $\{r_h, r_v\} = \{3000,50\}$ m and $\sigma_D = 0.02$ S m^{-1}. Figure 10a and c shows filled contours of $|E_z^a|^{\mathrm{IE}}$ as a function of location in D for $d = \{1000,2000\}$ m, respectively. Figure 10b and d shows filled contours of $|E_z^a|^{\mathrm{SIE}}$ as a function of location in D for $d = \{1000,2000\}$ m, respectively. The accuracy of the $\mathrm{SIE_{II}}$ method for $f = 0.1$ Hz is as good as in the base case. The dash-dot curves in Figure 10e and f show γ_z as a function of f and β, respectively, for $d = 1000$ m. The dashed curves in Figure 10e and f show γ_z as a func-

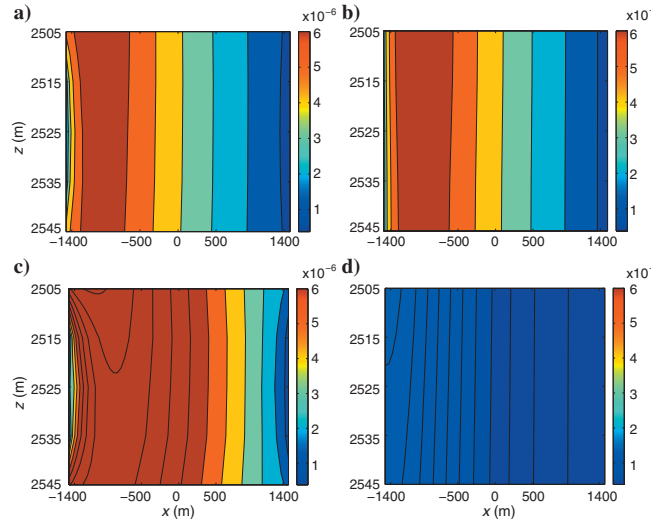

Figure 5. The amplitude $|E_z^a|$ as a function of location in D obtained by methods (a) IE, (b) SIE, (c) QL, and (d) QA, for $f = 0.1$ Hz, $\sigma_D = 0.02$ S m^{-1}, and $\sigma^b = 1$ S m^{-1}.

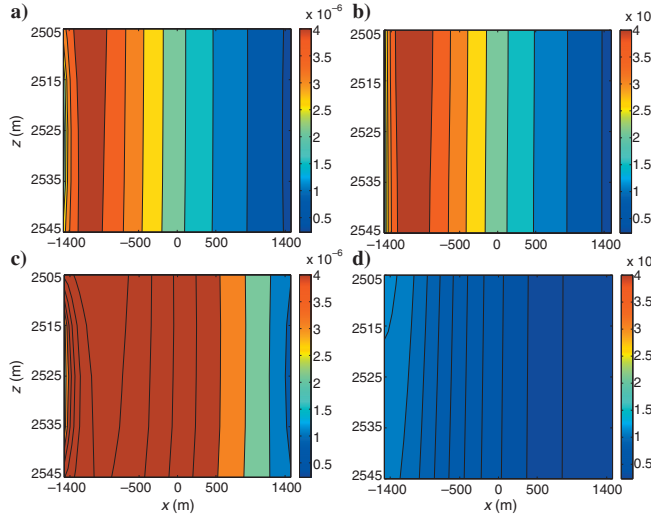

Figure 6. The amplitude $|E_z^a|$ as a function of location in D obtained by methods (a) IE, (b) SIE, (c) QL, and (d) QA, for $f = 0.1$ Hz, $\sigma_D = 0.05$ S m^{-1}, and $\sigma^b = 1$ S m^{-1}.

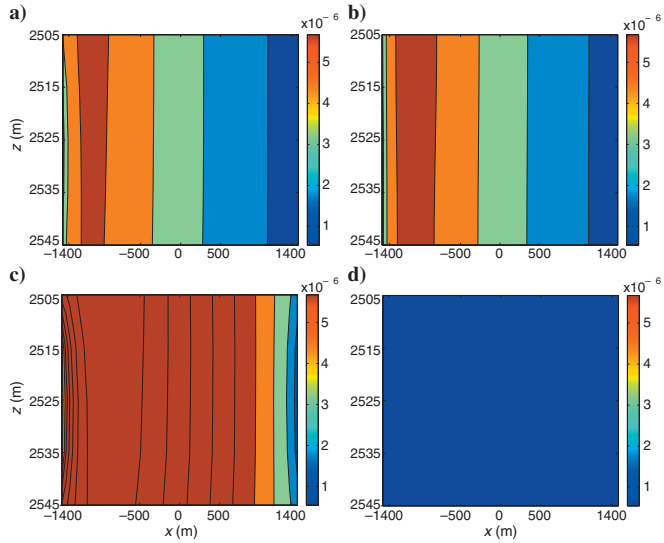

Figure 7. The amplitude $|E_z^v|$ as a function of location in D obtained by methods (a) IE, (b) SIE, (c) QL, and (d) QA, for $f = 0.1$ Hz, $\sigma_D = 0.02$ S m^{-1}, and $\sigma^b = 0.3$ S m^{-1}.

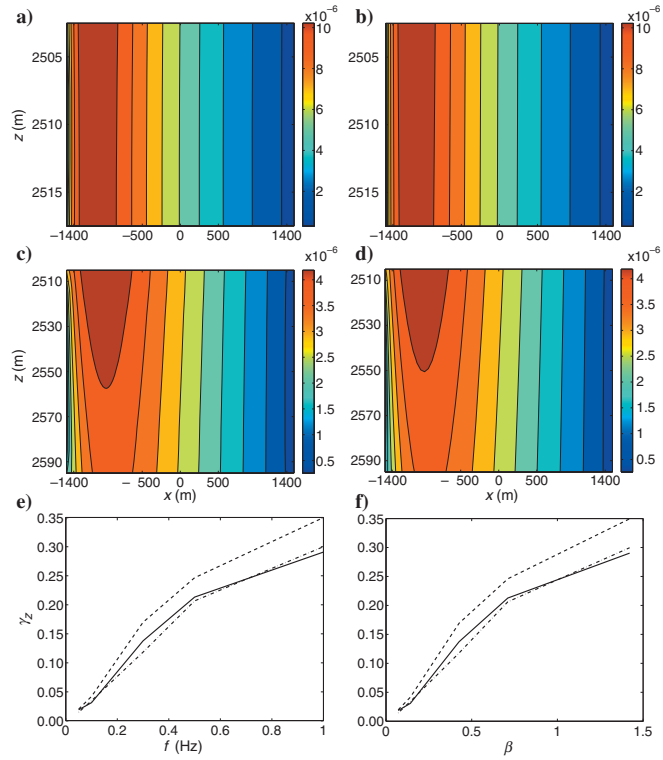

Figure 8. The amplitude $|E_z^v|$ as a function of location in D obtained by methods (a and c) IE, and (b and d) SIE. Perturbed vertical extension: (a and b) $r_v = 20$ m, (c and d) $r_v = 100$ m. In (a-d), $f = 0.1$ Hz. The mean relative error γ_z is shown as a function of (e) f and (f) β, respectively. Base case (solid lines), $r_v = 20$ m (dash-dot lines), $r_v = 100$ m (dashed lines).

tion of f and β, respectively, for $d = 2000$ m. The variation of γ_z with f and β is very similar to that in the base case. This is as expected because β does not depend on d.

(The case is included to demonstrate, also with numerical computations, that the accuracy of the SIE_{II} method is independent of d. We also have run examples with horizontally layered background conductivity. The results showed that the accuracy of the SIE_{II} method with respect to the rigorous IE method is as good as for a homogeneous background conductivity. Again, this is as expected because β [in setting II] does not depend on the background conductivity.)

Overall, the computational results with the SIE and rigorous IE methods confirm the preliminary conclusions that were drawn earlier just by examining values of β: the SIE_I method will not result in good approximations to the rigorous IE method, except for extremely low frequencies, and the SIE_{II} method will result in good approximations to the rigorous IE method for many frequencies and reservoir dimensions within the selected parameter ranges. In addition, the SIE_{II} method is significantly more accurate than the QL and QA approximations for these parameter ranges.

SUMMARY

We have presented a novel simplified integral equation (SIE) modeling approach. The approach is aimed at low frequencies and resistive targets, such as with marine CSEM for petroleum exploration. Rigorous integral equation (IE) modeling consists of three steps. The first step is to compute $\mathbf{E}^b$ in the anomaly D and in the receivers, and $\mathbf{H}^b$ in the receivers. The second is to compute $\mathbf{E}^a$ in D. The third is to compute $\mathbf{E}^a$ and $\boldsymbol{H}^a$ in the receivers. The second step is computationally very intensive for large problems because solving a linear system with a dense coefficient matrix is involved. We consider the use of a variable-coefficient Poisson's equation to circumvent the computationally intensive second step of rigorous IE modeling.

The SIE approach also consists of three steps. The first step is identical to that of the rigorous IE method. For the second and third steps, we consider two settings. In setting I, the Poisson's equation is used to compute $\boldsymbol{E}^a$ in D and in the receivers. The third step in setting

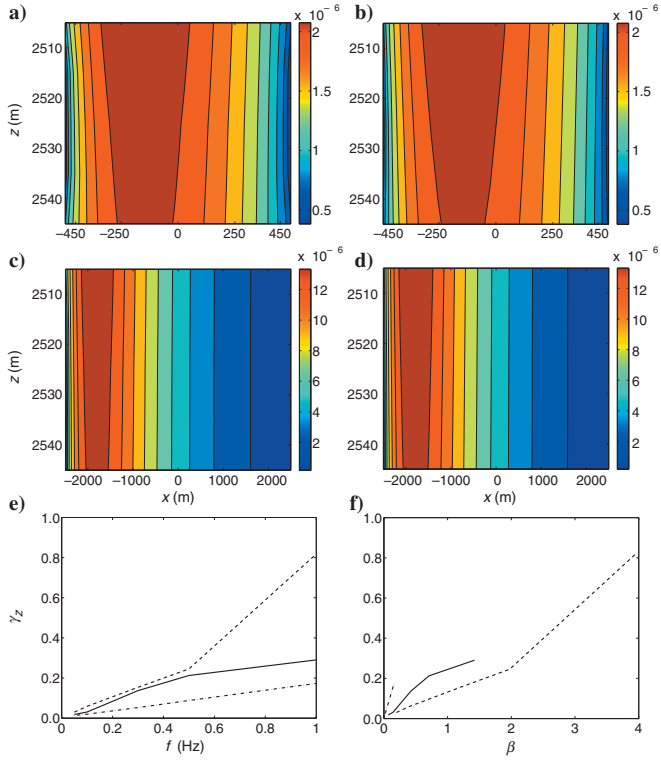

Figure 9. The amplitude $|E_z^a|$ as a function of location in D obtained by methods (a and c) IE, and (b and d) SIE. Perturbed horizontal extension: (a and b) $r_h = 1000$ m, (c and d) $r_h = 5000$ m. In (a-d), $f = 0.1$ Hz. The mean relative error γ_z is shown as a function of (e) f and (f) β, respectively. Base case (solid lines), $r_h = 1000$ m (dash-dot lines), $r_h = 5000$ m (dashed lines).

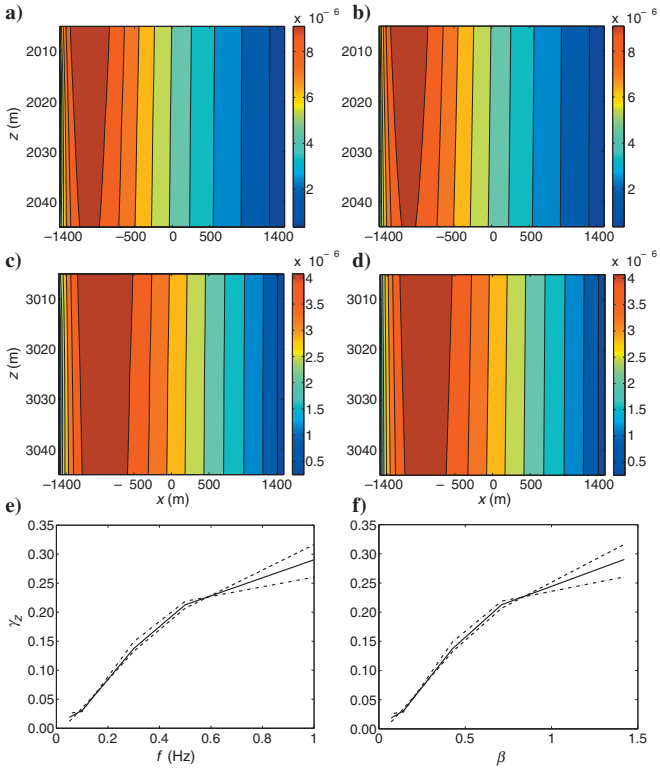

Figure 10. The amplitude $|E_z^a|$ as a function of location in D obtained by methods (a and c) IE, and (b and d) SIE. Perturbed depth below seafloor: (a and b) $d = 1000$ m, (c and d) $d = 2000$ m. In (a-d), $f = 0.1$ Hz. The mean relative error γ_z is shown as a function of (e) f and (f) β, respectively. Base case (solid lines), $d = 1000$ m (dash-dot lines), $d = 2000$ m (dashed lines).

I is to compute $\mathbf{H}^a$ in the receivers in the same manner as with the rigorous IE method. In setting II, the Poisson's equation is used to compute $\mathbf{E}^a$ in D only. The third step in setting II is to compute $\mathbf{E}^a$ and $\mathbf{H}^a$ in the receivers in the same manner as with the rigorous IE method. The accuracy of the SIE approach is assessed by order-of-magnitude calculations and by numerical comparisons of the SIE approach to the rigorous IE method for a selected range of parameter values. The SIE approach also is compared to the quasi-linear (QL) and quasi-analytic (QA) approximations.

CONCLUSIONS

Order-of-magnitude calculations and computational results with the SIE and rigorous IE methods show that, in setting I, the SIE approach will not result in good approximations to the rigorous IE method, except for extremely low frequencies and reservoirs at a fairly shallow depth.

In setting II, however, order-of-magnitude calculations and computational results show that the SIE approach will result in good approximations to the rigorous IE method for many frequencies and target dimensions within the selected parameter ranges. Relative differences between SIE results and rigorous IE results in D are below 25% for $f = 0.5$ Hz, and below 5% for $f = 0.1$ Hz. These relative differences are independent of reservoir depth and background conductivity. In addition, the SIE approach is significantly more accurate than the QL and QA approximations.

Based on these results for settings I and II, we recommend the use of the SIE approach in setting II only.

The variable-coefficient Poisson solver is in the process of being extended to three dimensions. A 3D Poisson solver will allow for a thorough comparison of computational efficiency between the SIE approach in setting II and the rigorous IE method. It will allow also for an extended comparison of accuracy between the SIE approach in setting II and the rigorous IE method, involving a larger set of conductivity models than those applied in the present study. These research topics will be pursued when the 3D Poisson solver is in place.

ACKNOWLEDGMENTS

The first author is grateful for the financial support of VISTA, a research cooperation between the Norwegian Academy of Science and Letters and StatoilHydro, to perform this study. The authors also gratefully acknowledge the Consortium for Electromagnetic Modeling and Inversion at the University of Utah for providing the IE code, INTEM3D.

REFERENCES

Best, M. E., P. Duncan, F. J. Jacobs, and W. L. Scheen, 1985, Numerical modeling of the electromagnetic response of three-dimensional conductors in a layered earth: Geophysics, **50**, 665–676.

Carazzone, J. J., O. M. Burtz, K. E. Green, and D. A. Pavlov, 2005, Three dimensional imaging of marine CSEM data: 75th Annual International Meeting, SEG, Expanded Abstracts, 575–578.

Chave, A. D., A. H. Flosadottir, and C. S. Cox, 1990, Some comments on the seabed propagation of VLF/ULF electromagnetic fields: Radio Science, **25**, 825–836.

Cheney, M., D. Isaacson, and J. C. Newell, Electrical impedance tomography: SIAM Review, **41**, 85–101.

Constable, S., and C. S. Cox, 1996, Marine controlled-source electromagnetic sounding: 2 — The PEGASUS experiment: Journal of Geophysical Research, **101**, 5519–5530.

Cox, C. S., S. C. Constable, A. D. Chave, and S. C. Webb, 1986, Controlled-source electromagnetic sounding of the oceanic lithosphere: Nature, **320**, 52–54.

Cox, C. S., J. H. Filloux, and J. Larsen, 1971, Electromagnetic studies of ocean currents and electrical conductivity below the ocean floor, *in* A. Maxwell, ed., The sea, vol. 4: Wiley 637–693.

Eidesmo, T., S. Ellingsrud, L. M. MacGregor, S. Constable, M. C. Sinha, S. Johansen, F. N. Kong, and H. Westerdahl, 2002, Sea bed logging (SBL), a new method for remote and direct identification of hydrocarbon filled layers in deepwater areas: First Break, **20**, 144–152.

Ellingsrud, S., T. Eidesmo, S. Johansen, M. C. Sinha, L. M. MacGregor, and S. Constable, 2002, Remote sensing of hydrocarbon layers by seabed logging (SBL), Results from a cruise offshore Angola: The Leading Edge, **21**, 972–982.

Evans, R. L., M. C. Sinha, S. Constable, and M. J. Unsworth, 1994, On the electrical nature of the axial melt zone at 13N on the East Pacific Rise:

Journal of Geophysical Research, **99**, 577–588.
Gupta, P. K., L. A. Bennett, and A. P. Raiche, 1987, Hybrid calculations of the three-dimensional electromagnetic response of buried conductors: Geophysics, **52**, 301–306.
Hesthammer, J., and M. Boulaenko, 2005, The offshore EM challenge: First Break, **23**, 59–66.
Hursán, G., and M. S. Zhdanov, 2002, Contraction integral method in three-dimensional electromagnetic modeling: Radio Science, **37**, 1089.
Lee, K. H., D. F. Pridmore, and H. F. Morrison, 1981, A hybrid three-dimensional electromagnetic modeling scheme: Geophysics, **46**, 796–805.
MacGregor, L. M., and M. C. Sinha, 2000, Use of marine controlled source electromagnetic sounding for sub-basalt exploration: Geophysical Prospecting, **48**, 1091–1106.
Srnka, L. J., J. J. Carazzone, M. S. Ephron, and E. A. Eriksen, 2005, Remote reservoir resistivity mapping — An overview: 75th Annual International Meeting, SEG, Expanded Abstracts, 569–571.
Tompkins, M. J., 2004, Marine controlled-source electromagnetic imaging for hydrocarbon exploration: Interpreting subsurface electrical properties: First Break, **22**, 45–51.
Young, P. D., and C. S. Cox, 1981, Electromagnetic active source sounding near the East Pacific Rise: Geophysical Research Letters, **8**, 1043–1046.
Zhdanov, M., 2002, Geophysical inverse theory and regularization problems: Elsevier.
Zhdanov, M. S., V. I. Dmitriev, S. Fang, and G. Hursan, 2000, Quasi-analytical approximations and series in electromagnetic modeling: Geophysics, **65**, 1746–1757.
Zhdanov, M. S., and S. Fang, 1996, Quasi-linear approximation in 3D electromagnetic modeling: Geophysics, **61**, 646–665.